# Emergence of ferromagnetism through the metal-insulator transition in undoped indium tin oxide films

Samuel Mumford, Tiffany Paul, and Aharon Kapitulnik

Phys. Rev. Materials **5**, 125201 — Published 3 December 2021

DOI: 10.1103/PhysRevMaterials.5.125201

# Emergence of Ferromagnetism Through the Metal-Insulator Transition in Undoped Indium Tin Oxide Films

Samuel Mumford,[1,2,*] Tiffany Paul,[1,3,*] and Aharon Kapitulnik[1,2,3]

[1]*Geballe Laboratory for Advanced Materials, Stanford University, Stanford CA, 94305, USA*
[2]*Department of Physics, Stanford University, Stanford CA, 94305, USA*
[3]*Department of Applied Physics, Stanford University, Stanford CA, 94305, USA*
(Dated: October 19, 2021)

We present a detailed study of the emergence of bulk ferromagnetism in low carrier density samples of undoped indium tin oxide (ITO). We used annealing to increase the density of oxygen vacancies and change sample morphology without introducing impurities through the metal insulator transition (MIT). We utilized a novel and highly sensitive "Corbino-disk torque magnetometry" technique to simultaneously measure the thermodynamic and transport effects of magnetism on the same sample after successive annealing. With increased sample granularity, carrier density increased, the sample became more metallic, and ferromagnetism appeared as resistance approached the MIT. Ferromagnetism was observed through the detection of magnetization hysteresis, anomalous Hall effect (AHE), and hysteretic magnetoresistance. A sign change of the AHE as the MIT is approached may elucidate the interplay between the impurity band and the conduction band in the weakly insulating side of the MIT. [a]

## I. INTRODUCTION

The initial discovery of room-temperature ferromagnetism in Co-doped $TiO_2$ [1] films was soon followed by the observation of similar behavior in other transition-metal (TM) doped oxides including Co-doped $SnO_2$ [2], Mn-doped ZnO [3], Co-doped $CeO_2$ [4], and Ni, Mo, Fe, and Mn-doped $In_2O_3$ [5–8]. The origin of the observed thin film magnetism continues to be debated, particularly after the discovery of ferromagnetism in undoped oxides such as $HfO_2$ [9], $TiO_2$, and $In_2O_3$ [10]. At the heart of the puzzle is observation that the respective bulk undoped oxides exhibit only diamagnetism. Similarly, doping level in TM doped oxides was often too low to explain the observed strength, anisotropy, or thermal treatment sensitivity of the magnetic state. Correlation between the samples' morphology and the occurrence of magnetism instead suggests an explanation based on a spontaneous formation of defects or oxygen vacancies [10]. The abundant surface vacancies of the nanoparticles which make up a granular structure provide unpaired electron spins which could interact via an exchange mechanism [11].

With the observation of ferromagnetism in $In_2O_3$ and $SnO_2$, it is natural to explore whether the widely used solid-solution of tin-doped indium oxide (ITO) exhibits ferromagnetism. Ferromagnetism could be used to integrate this optoelectronic material into novel spintronics applications. Indeed, various TM doped [6, 12–15] and undoped [5, 16, 17] ITO systems were shown to exhibit ferromagnetism that persisted to room temperature. Oxygen vacancy defects have been proposed as the source of magnetic moments rather than impurities [17–19], while itinerant carriers mediate the collective ferromagnetic state [15, 16, 20]. A persistent obstacle in proclaiming intrinsic ferromagnetism for ITO has been the difficulty in observing the anomalous Hall effect (AHE) and hysteretic magnetoresistance. For example, in Cr-doped ITO AHE appears only at very high carrier concentrations exceeding $10^{21}$ cm$^{-3}$ [15], while in 12% Co-doped ITO (10% Sn) AHE appears above $\sim 10^{19}$ cm$^{-3}$. Samples of ITO with lower concentrations of magnetic elements generally do not show AHE, and the observed negative magnetoresistance is attributed to magnetic-field induced reduction in spin scattering [15, 19, 20]. Similar to other magnetic semiconductors (e.g. [21]), ITO is a heavily doped *n*-type semiconductor typically studied near the metal-insulator transition (MIT). In particular, undoped ITO close to the MIT may exhibit local magnetic moments that are typically self-generated in quenched disordered electronic systems due to interaction effects [22]. Thus carrier density may not be the only relevant parameter for magnetism [20, 23]. It is correspondingly important to elucidate the occurrence of ferromagnetism in undoped ITO within these contexts.

In this work we examine the interplay between morphology, proximity to the MIT, and the emergence of bulk magnetic properties in low carrier density samples of ITO. We used annealing to increase the density of oxygen vacancies and change sample granularity without introducing impurities [24–31]. Annealing reduced resistivity and was performed across the MIT. We utilized a novel and highly sensitive "Corbino disk torque magnetometry" technique to simultaneously measure the thermodynamic and transport effects of magnetism on the same sample after successive annealing. Our results clearly show that: *i*) Starting with a highly insulating mostly amorphous ITO with no observed magnetism, successive annealing induces morphology change towards more granular structure. This change is accompanied by increase in carrier density and occurrence of ferromagnetism near the MIT. *ii*) The amplitude of magnetization hysteresis and saturating field both increase with decreased in sheet-resistance, indicating strengthening of the ferromagnetic state. *iii*) Undoped ITO thus is ferromagnetic, exhibiting anomalous Hall effect and hysteretic magnetoresistance for carrier density as low as $\approx 3\times 10^{18}$ carriers/cm$^3$. *iv*) Both AHE and hysteretic magnetoresistance are observed across the MIT. The sign of

[*] These authors contributed equally to this article.
[a] Corresponding author is Samuel Mumford at smumfor2@stanford.edu

AHE changes from negative on the insulating side of the MIT to positive AHE on the metallic side of the MIT.

## II. EXPERIMENT

### A. Preparation of Samples

Hall bar and Corbino disk patterned ITO samples were prepared by RF magnetron sputtering using a 10% Sn target at 8 W/Inch$^2$, 5 mTorr of Ar pressure, and 2.5% partial pressure of $O_2$. Both Hall bar and Corbino disk samples were subjected to successive annealing schedules at 400 K and pressure of $< 10^{-5}$ Torr with measurements performed after each multi-day anneal. A typical ITO sample was initially highly insulating and exhibited a starting sheet resistance of 70 k$\Omega/\square$ at room temperature and a thickness of 40 nm. Resistance increased to 460 k$\Omega/\square$ at the measurement base temperature of 4.2 K. Measurements were performed in a liquid helium cryostat with a 7 T superconducting magnet. Hall effect and magnetoresistance were measured on the Hall bars using standard 5 lead configuration. The Corbino disk samples were measured by torque magnetometry as described below.

### B. Corbino Disk Torque Magnetometry

Cantilever torque magnetometry utilizes a high-$Q$ resonator to detect the interaction between a magnetic dipole $\vec{\mu}$ and an external magnetic field $\vec{B}$ [32–36], where the resulting torque is [34]

$$\vec{\tau} = \vec{\mu} \times \vec{B}. \tag{1}$$

A schematic depiction of cantilever torque magnetometry is shown in Fig. 1(a). The angular response $\theta$ of a cantilever with moment of inertia $A$, resonant frequency $\omega_0$, and quality factor $Q$ subject to an external torque $\tau$ may be approximated as a damped harmonic oscillator following [37]

$$A\ddot{\theta} + \frac{A}{Q}\omega_0\dot{\theta} + A\omega_0^2\theta = \tau. \tag{2}$$

The torque of a dipole parallel to the cantilever surface norm and a static $z$-aligned magnetic field $B$ shifts resonant frequency as

$$A\omega_0^2 \rightarrow A\omega_0^2 - \mu B, \quad \text{or} \quad \frac{\Delta\omega_0}{\omega_0} = \frac{\mu B}{2A\omega_0^2}. \tag{3}$$

The circulating current in a Corbino disk [38] patterned on a cantilever forms such a magnetic dipole parallel to the cantilever surface norm [32]. Silicon cantilevers of dimension $200 \times 600 \times 3$ $\mu$m were fabricated with Corbino disks as shown in Fig. 1(b). The resulting devices exhibited $A = 3 \times 10^{-18}$ kg-m$^2$ and $f_0 = \omega_0/2\pi = 14.616$ kHz. Finally, the cantilever resonant frequency was observed interferometrically and driven through laser radiation pressure [32].

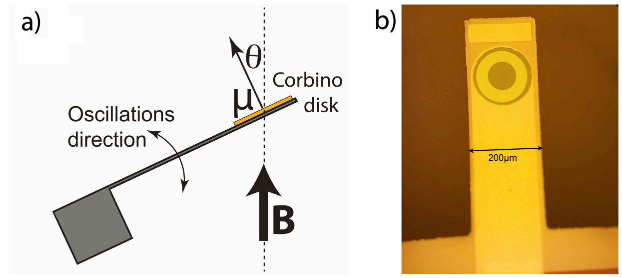


FIG. 1: (a) Schematic of torque magnetometry where Hall currents in a Corbino disk induce the magnetic moment $\mu$, adapted from [32]. (b) Picture of the ITO Corbino disk cantilever. The center contact is connected to an underlying ground plane. The metal pad on the end of the cantilever is used for optical alignment.

Cantilevers with ITO Corbino disks were examined for magnetization and magnetic transport effects. Sample magnetization is measured through the voltage-independent shift in resonant frequency

$$\Delta f_0(B) = f_0(B) - f_0(B=0). \tag{4}$$

Sample transport properties for Corbino disk voltage $V$ are measured through the voltage-dependent shift

$$\delta f_0(\pm V, B) = f_0(+V, B) - f_0(-V, B). \tag{5}$$

The Hall effect is measured through the even in $B$ component of $\delta f_0(\pm V, B)$ while the odd component of $\delta f_0(\pm V, B)$ is caused by contact misalignment and longitudinal current. As shown by Mumford *et al.* [32], using Eqn. 3 the even component of $\delta f_0(\pm V, B)$ yields Hall conductivity

$$\sigma_{xy} = C\frac{\delta f_0}{BV}, \text{ where } C = \frac{4Af_0 \ln(r_o/r_i)}{\pi(r_o^2 - r_i^2)} \tag{6}$$

and $r_o$ and $r_i$ are the outer and inner radii of the disk. Thus, $\delta f_0(\pm V, B)$ is proportional to $\sigma_{xy}B$ and the expected Hall contribution to $\delta f_0$ is proportional to $B^2$ for $\sigma_{xy} \propto B$. The quadratic dependence of the even component of $\delta f_0(\pm V, B)$ and the extraction of Hall conductivity for a nonmagnetic sample are shown in Fig. 2.

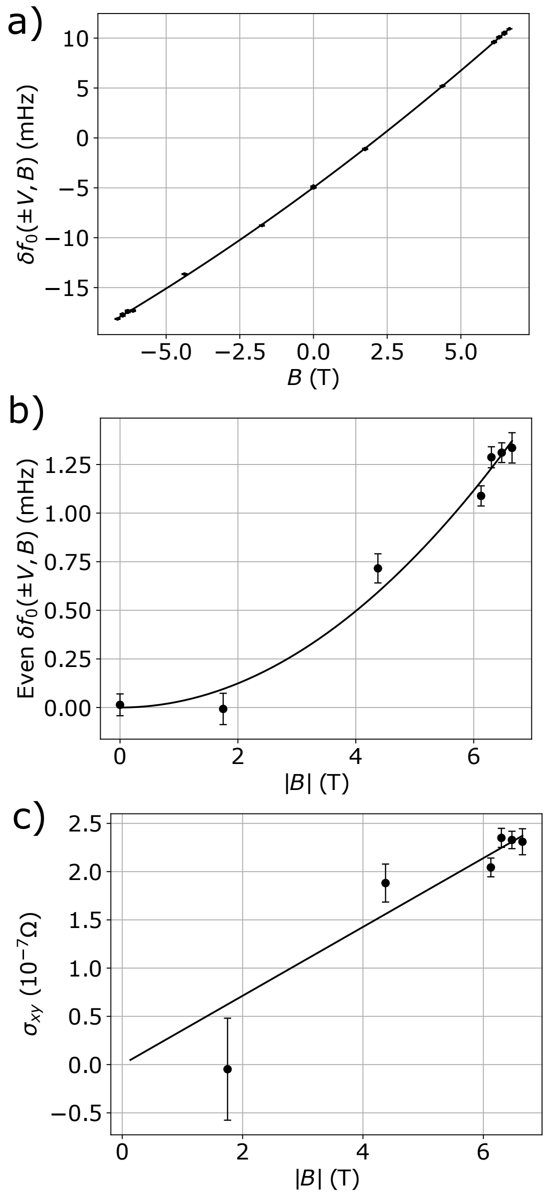


FIG. 2: Example of extracting the even component of $\delta f_0(\pm V, B)$ and $\sigma_{xy}$ for non-magnetic metallic ITO, adapted from [32]. (a) A full dataset of $\delta f_0(\pm V, B)$ including the linear in $B$ term in $\delta f_0(\pm V, B)$ due to misalignment. (b) The even component of $\delta f_0(\pm V, B)$ found by averaging $\delta f_0(\pm V, -B)$ and $\delta f_0(\pm V, +B)$. (c) Extracted Hall conductivity from the even component of $\delta f_0(\pm V, B)$ and Eqn. 6.

## III. RESULTS AND DISCUSSION

### A. Characterization of Samples

ITO grain size and granularity increased with annealing as shown in Fig. 3. As deposited, the ITO was largely amorphous with a smooth surface profiled by atomic force microscopy (AFM). After annealing, the ITO subdivided into grains with height fluctuations nearly equal to the deposited ITO thickness as seen in Fig. 3(a-b). Complimentary scanning electron microscope (SEM) images also demonstrate a change in granularity with annealing. Two samples of ITO were analyzed by SEM. Sample 1 was patterned in a Hall bar (a-b/c-d) and sample 2 was patterned in a Corbino disk (e-f). As deposited in a Hall bar, the ITO exhibited an amorphous structure, with only stripes and SEM noise seen in Fig. 3(a) and (c). The unannealed Corbino disk ITO shown in Fig. 3(e) instead exhibits large grains. The differences between the as-deposited ITO in the Corbino disk and Hall bar may be explained by a difference in deposited ITO morphology based on substrate [39], or by partial annealing of the Corbino disk ITO during cantilever plasma etching. After annealing, the ITO became granular with typical grain size on the order of 500 nm$^2$ in both sample geometries. The convergence of grain geometries by image grain detection is shown in Fig. 9 in App. A. The sheet resistance at base temperature also decreased with annealing, while the carrier density increased as is shown in Table I. Such a change in grain size [24–30], decreased resistivity, and increased carrier density [24, 26–28, 31] are consistent with previous observations on ITO with higher temperature thermal annealing.

| Resistivity ($k\Omega/\square$) | Configuration | $n$ ($10^{18}$ cm$^{-3}$) |
|---|---|---|
| 3300 | Corbino Disk | -0.08 ± 0.2 |
| 460 | Corbino Disk | 0.17 ± 0.04 |
| 185 | Corbino Disk | 1.7 ± 1 |
| 48 | Corbino Disk | 3.4 ± 0.5 |
| 32 | Corbino Disk | -2.7 ± 0.3 |
| 17 | Corbino Disk | 6.5 ± 1.4 |
| 15 | Hall Bar | 9.33 ± 0.02 |
| 8.5 | Corbino Disk | 22 ± 10 |
| 4.6 | Hall Bar | 23.7 ± 0.1 |

TABLE I: Samples investigated in this study and their transport properties at base temperature.

### B. Corbino Disk Torque Magnetometry of ITO

#### 1. *Hall Conductivity Annealing Across MIT*

An initially highly resistive ITO cantilever (resistivity of 3300 k$\Omega/\square$ at base temperature) was annealed in 6 steps to investigate the variation of Hall conductivity through the MIT as well as the onset and evolution of magnetism. Fig. 4(a) shows the measured Hall conductivity at 5 T of an ITO sample with annealing, while the respective carrier densities are given in Table I. Annealed Hall-bar configuration samples are included for comparison. Ferromagnetism emerged close to the MIT and thus complicated extracting the ordinary Hall effect from $\delta f_0(\pm V, B)$ as discussed in further detail below. This increased complexity increases the uncertainty in $\sigma_{xy}$ extracted near and below the MIT, but the observed carrier densities remain consistent with similarly prepared samples measured in a Hall bar configuration.

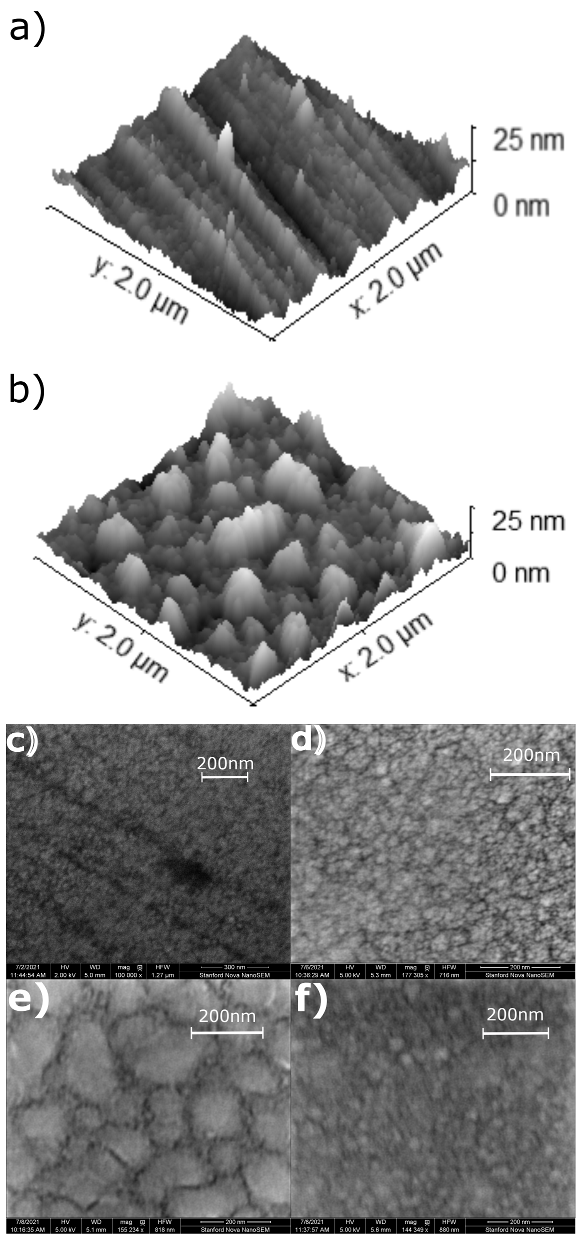


FIG. 3: Characterization of the granularity of ITO with annealing. The initially large patches of ITO or smooth ITO breaks down into granular areas after annealing. (a-b) AFM profile of ITO Hall bar before and after annealing. Sample height fluctuations and granularity increase after annealing. (c-d) SEM images of ITO Hall bar before and after annealing. (e-f) SEM images of Corbino disk ITO before and after annealing.

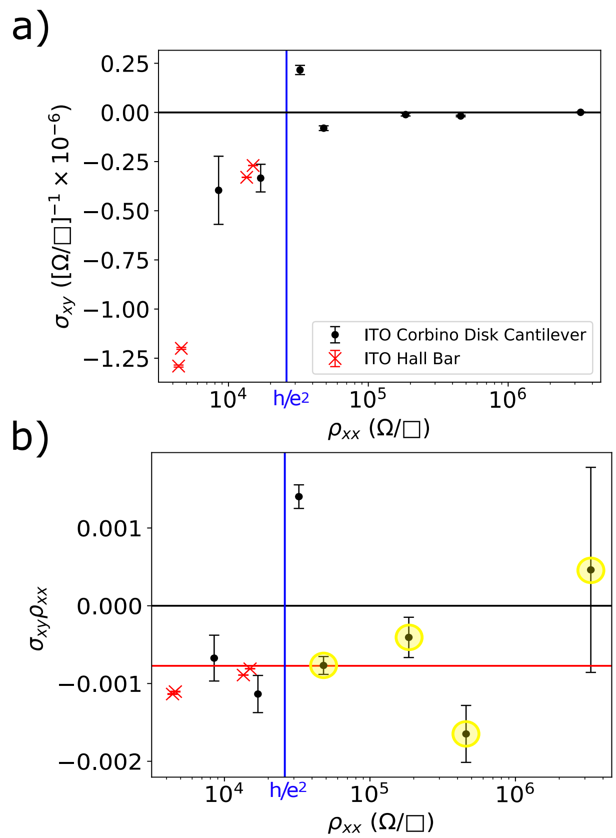


FIG. 4: Behavior of $\sigma_{xy}$ and $\sigma_{xy}\rho_{xx}$ at 5 T measured on a series of annealed ITO samples through the MIT. The outlying sample very close to the MIT may be strongly influenced by the magnetic behavior as discussed in Secs. III B 2-III B 3. Additional data obtained through a Hall bar approach and discussed in Sec. III C is included as a reference. Resistive and non-magnetic points above the MIT are highlighted in (b).

An important result to be drawn from the high resistance samples deep in the hopping regime is the tendency of $\sigma_{xy}$ to vanish with increasing disorder or increasing $\rho_{xx}$. The hopping regime Hall effect is governed by the self-interference effect of the electron wave function propagating along limited paths dictated by magnetic field and the impurity sites responsible for the impurity band. Early theoretical work by Friedman and Pollak [40] using the Holstein approach [41] concluded that the Hall resistivity diverges as the temperature tends to zero. This result was then reinforced by Entin-Wohlman, *et al.* [42], who attempted to explain the discrepancy with complementary calculations predicting an electronic state where the longitudinal resistance diverges at zero temperature, but the Hall resistivity remains constant [43–45]. Such a state is known as a Hall insulator. Indeed, while experimental results focused on the vicinity of the MIT confirmed divergence of $\rho_{xy}$ on the insulating side [46, 47], in other experiments insulating states derived from quantum Hall states were consistent with a Hall insulator. The result for $\rho_{xy}$ may be different depending on the order of temperature and frequency limits taken in the DC limit of the Hall resistivity. Similarly, it was emphasized in [42] that if both $\rho_{xy}$ and $\rho_{xx}$ are calculated and averaged over the disorder, they should both show divergence, while if the respective conductivities are averaged over the disorder the calculated $\rho_{xy}$ may approach a constant. We directly measure $\sigma_{xy}$ and $\rho_{xx}$, which is a hybrid of the above two procedures.

| Resistivity (kΩ/□) | $B_S$ (T) | $\alpha$ (mHz/T$^2$) |
|---|---|---|
| 32 | 3±0.1 | 3.6±0.7 |
| 17 | 3.6±0.1 | 5.4±0.5 |
| 8.5 | 6±0.2 | 3.1±0.3 |

TABLE II: Hysteretic magnetization fit coefficients obtained through torque magnetometry. Magnetization was more pronounced as $B_s$ increased with increased annealing and lower resistance

We show $\sigma_{xy}\rho_{xx}$ in Fig. 4(b) to test the Hall behavior. The observed $\sigma_{xy}\rho_{xx}$ is approximately a constant, excluding the very vicinity of the MIT. Far above the MIT weak localization corrections may alter the ratio [47] at a level smaller than the resolution of the experiment. However, on the insulating side, a Hall insulating behavior would require that $\sigma_{xy}\rho_{xx} \sim \rho_{xx}^{-1}$ in contrast to the observed behavior. A constant $\sigma_{xy}\rho_{xx}$ supports that in ITO above the MIT $\rho_{xy} \propto \rho_{xx}$. Such behavior would be expected if $\rho_{xx}$ and $\rho_{xy}$ both diverge as $1/n$ for thermally activated carrier density $n$ as $T \to 0$.

### 2. *Magnetism Near MIT*

Successive annealing of highly insulating ITO resulted in increased granularity, lower resistivity, and the emergence of ferromagnetism as the MIT was approached. We now profile the origin of the surprising magnetism, as well as its anisotropy and dependence on the film morphology, carrier density, and defect density.

Anisotropy in bulk magnetization may be observed through cantilever torque magnetometry [33–36]. Hysteresis in magnetization due to ferromagnetic ordering results in hysteresis in $\Delta f_0(B)$ observed through Eqns. 3 and 4. Ferromagnetic hysteresis in $\Delta f_0(B)$ appeared after annealing near the MIT point as shown in Fig. 5. All tested cantilevers with patterned metallic layers displayed low-field shifts in $f_0$ as discussed in Appendix B, thus only the hysteresis in magnetization for $|B| > 1.5$ T can be attributed to sample magnetization. The amplitude of the magnetic hysteresis loop increased with annealing and confirms that the observed $\Delta f_0$ hysteresis arose from changes in the ITO. To rule out systematic factors, the order of data-taking was switched between the two 32 kΩ/□ datasets, and a 6 hour delay at +7 T was inserted between the sweep up and sweep down runs of the 17 kΩ/□ dataset. The lack of hysteresis at high magnetic field confirms that hysteresis in $\Delta f_0(B)$ arose from changes in the ITO instead of systematic factors. No hysteresis in magnetization was found for ITO with sheet resistance > 32 kΩ/□.

Magnetization hysteresis or hysteresis in $\Delta f_0$ above 1.5 T was fit to $\Delta f_{0,hyst} = \alpha(B - B_S)B$ for saturating field $B_S$ and proportionality constant $\alpha$. Fit coefficients are provided in Table II. The amplitude of magnetization and $B_S$ increased with annealing, as previously observed in ITO [16]. Note that stronger $z$-axis magnetism raises $f_0$, while in-plane magnetism can decrease $f_0$. The lower $f_0$ during the ramp down in magnetic field is thus consistent with in-plane ferromagnetism. In-plane ferromagnetism has been observed previously in ITO and a $B_s \approx 2$ T for the more lightly annealed samples is consistent with previous observations of ferromagnetic ITO at room temperature [5]. However, the coercive field of ITO can vary between samples by a factor of $\approx 10$ [5, 16, 17] and increases with annealing.

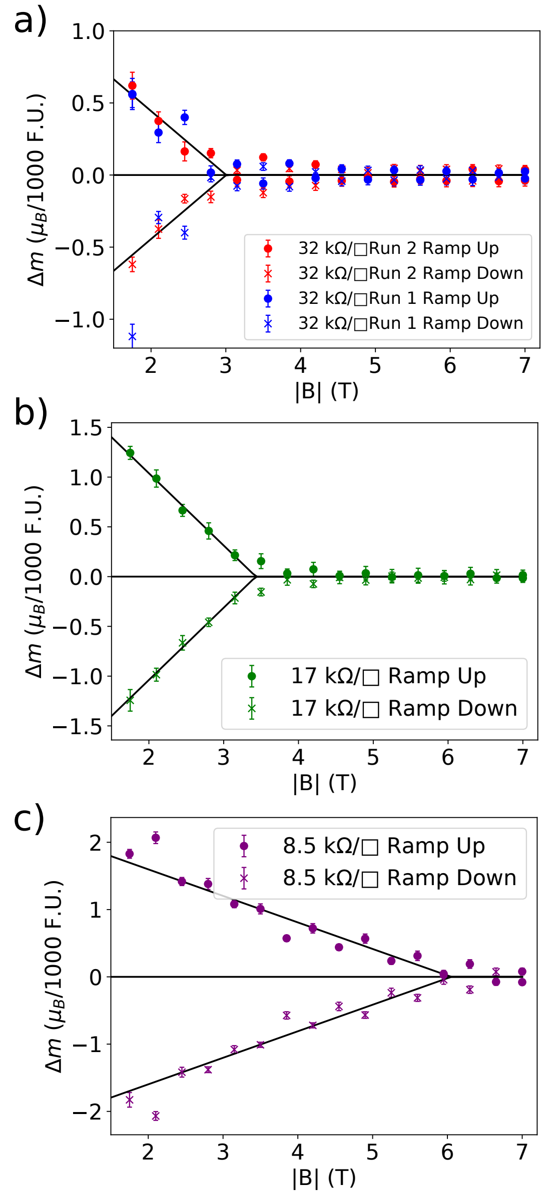


FIG. 5: Hysteresis in magnetization $\Delta m$ for three annealed ITO resistivities. We calculate the hysteretic magnetic moment per "formula unit" (f.u.), approximated as the unit cell volume of crystalline $In_2O_3$. The amplitude of hysteresis and saturating field increase with with longer annealing as shown in Table II. Ramping in magnetic field to ± 7 T was performed in 0.7 T steps.

The most annealed 8.5 kΩ/□ sample displayed a hysteretic magnetization saturating at $\Delta m \approx 0.002\mu_B$/f.u. where f.u. is the $In_2O_3$ unit cell volume. If we assume that the associated moment with each defect is of order $\sim 1\mu_B$, we obtain an approximate magnetic defect density of $1.3\times10^{19}$ defects/cm$^3$, within a factor of 2 of the carrier density shown in Table I. However, the large anisotropy field, the presence of magnetism in thin films and nanoparticles of ITO and other oxides which is absent in the bulk [11], and annealing dependence of magnetism suggest [16] that the relevant magnetic properties are derived from the sample surface [11]. Oxide surface vacancy-based magnetism could be enhanced with the granular transition shown in Fig. 3. If we distribute the moments only at the surface of the film, and assume that because of surface roughness the effective surface area is increased by a factor of two, we obtain a surface magnetization of $\sim 0.1\ \mu_B$/f.u.. One out of 10 unit cells at the surface introduces a magnetic moment if each surface defect produces $\sim 1\mu_B$. Finally, the anisotropy energy $K_u$ can be approximated from the saturation magnetization and field. The approximate $K_u = B_s\Delta m_s/2 \approx 2\times10^4$ J/m$^3$ is about 10 times smaller than a typical anisotropy energy of a thin film of polycrystalline ferromagnetic $Fe_3O_4$ of similar thickness [48].

### 3. *Anomalous Hall Conductivity Near MIT*

The most direct demonstration of intrinsic ferromagnetism is the emergence of the anomalous Hall effect in the transverse channel. For a material with $z$-component of magnetization $M_z$ and coefficients $a$ and $b$,

$$\sigma_{xy} = aB + bM_z \to \delta f_0(\pm V, B) \propto B^2 + \beta B M_z. \qquad (7)$$

Using Corbino disk torque magnetometry, we can detect both the Hall and anomalous Hall effects. However, unlike a standard Hall bar configuration, the sample is voltage-biased and transverse conductivity $\sigma_{xy}(B)$ is directly measured by the magnetic moment created by circulating Hall currents.

There is clear evidence of nonlinear $\sigma_{xy}$ or the anomalous Hall effect in even component of $\delta f_0(\pm V,B)$. The extracted and fit $\sigma_{xy}$ from $\delta f_0(\pm V,B)$ is shown in Fig. 6. The even component of $\delta f_0(\pm V,B)$ is fit to Eqn. 7 assuming a diamagnetic sigmoidal $M_z$ with fit coefficients $a$ and $b$

$$M_z = \frac{a}{e^{(B_s - B)/b} + 1} \qquad (8)$$

appearing at the $B_s$ listed in Table II. An in-plane ferromagnet in out of plane field should exhibit $M_z = 0$ at $B_z = 0$. The initial in-plane magnetization cants to the $z$-axis as $B_z$ increases and saturates for $B_z > B_s$. A sigmoidal $M_z$ with $B_s >> b$ replicates this behavior while minimizing free fit parameters. The anomalous Hall signal can be seen in Fig. 6 both in the agreement to the fit form of Eqn. 7 and by noting that a linear extrapolation of the high field $\sigma_{xy}$ does not intersect $\sigma_{xy} = 0$ at $B = 0$. This is in contrast with the linear $\sigma_{xy}$ shown in Fig. 2. Finally, the region of varying anomalous Hall signal corresponds with the hysteresis loop bounds shown in Fig. 5 as expected.

We further comment on the sign change of the 32 kΩ/□ sample Hall conductivity shown in Fig. 6(a). Here we note that this sample was close to but on the insulating side of the MIT and thus at the onset the hopping regime. A sign change of the anomalous Hall effect is then possible as a function of the impurity band filling [23]. As our films experienced strong variations in oxygen vacancies and defects as the morphology changed through annealing, such an effect may be anticipated. Indeed, such sign reversal was previously observed in $(In_{0.27}Co_{0.73})_2O_{3-v}$ ($v$ denotes the oxygen vacancies) ferromagnetic semiconductors [49] in the variable range hopping regime, particularly as the temperature was reduced and localization effects dominate. As materials like ITO are based on the $In_2O_3$ oxide system where oxygen vacancies and morphology contribute to the creation of the impurity band, the observation of sign change in our ITO samples may have the same origin.

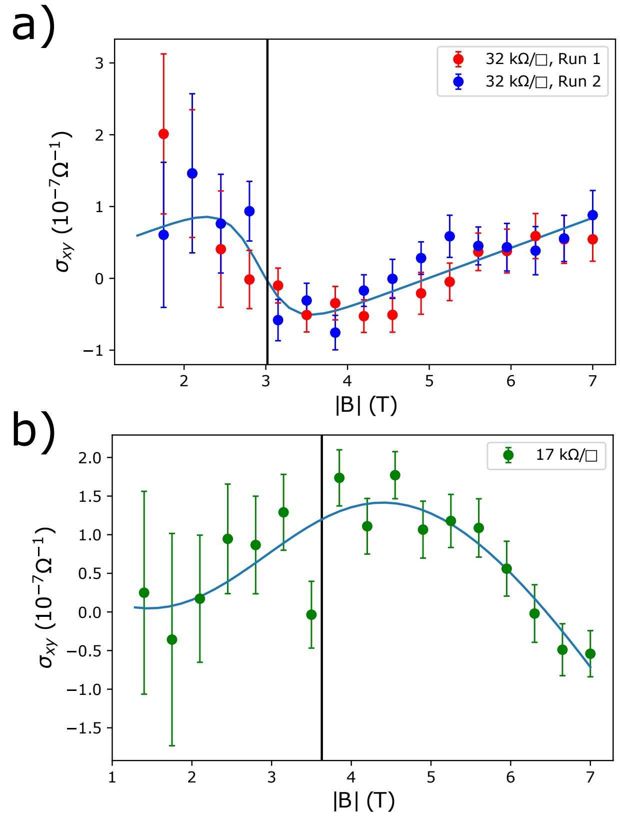


FIG. 6: Fits to the even component of $\delta f_0(\pm V,B)$ assuming a sigmoidal kink in anomalous Hall signal at $B_s$. For comparison, $B_s$ as fit from the closing of the $\Delta f_0$ hysteresis in Fig. 5 is shown with a vertical line. Low field cutoffs are imposed to avoid obscuring data with high errorbar points.

### 4. *Hysteretic Transport*

The detection of AHE is also accompanied by hysteresis in $\delta f_0(\pm V,B)$. As shown in Fig. 7, there is a hysteretic component of $\delta f_0(\pm V,B)$ with peaks coinciding with the closing of the $f_0$ hysteresis loops. The smoothly varying non-hysteretic component of $\delta f_0(\pm V,B)$ is the average between the up and

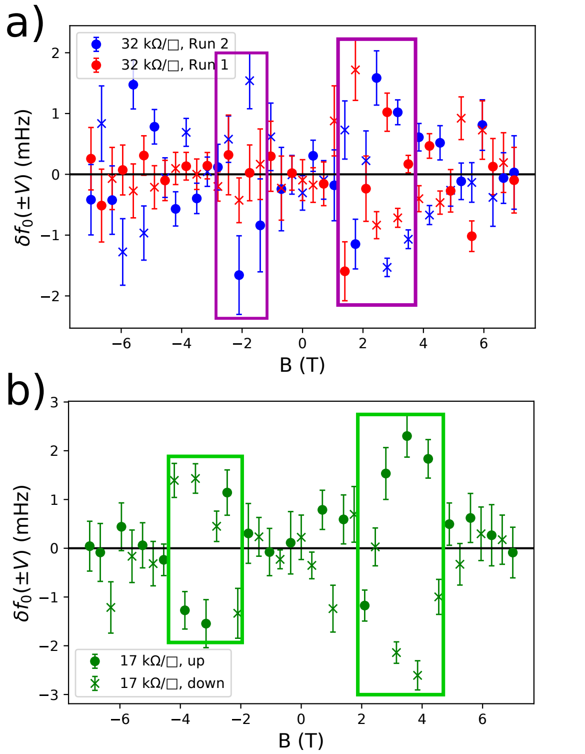


FIG. 7: Hysteresis in transport or $\delta f_0(\pm V,B)$ for 32 k$\Omega/\square$ and 17 k$\Omega/\square$ annealed devices. Peaks near the closing of the hysteresis loops are highlighted in boxes. The Corbino disk voltage was $\pm 0.3$ V. Hysteresis could appear due to both magnetoresistance for $B \lesssim B_s$ and the anomalous Hall effect as $B \approx B_s$.

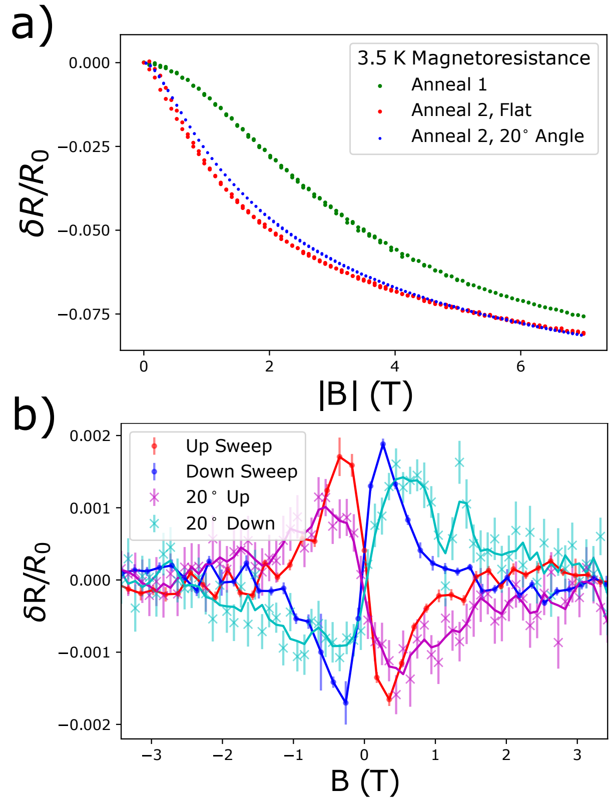


FIG. 8: (a) Magnetoresistance for a lightly annealed and more strongly annealed ITO sample. (b) Hysteresis in magnetoresistance after two stages of annealing for a vertically and 20° mounted Hall bar.

down magnetic field sweep values of $\delta f_0(\pm V,B)$ and is used to extract Hall conductivity and magnetoresistance. The hysteretic component of $\delta f_0(\pm V,B)$ is the difference between the smoothly varying background and $\delta f_0(\pm V,B)$ in each sweep direction. Hysteresis in transport closes above $B_S$ and qualitatively peaks near $B_S$ for annealed magnetic ITO cantilever datasets. The hysteretic $\delta f_0(\pm V,B)$ is approximately 0 at low field, although such a closing may be due to the lack of dipole sensitivity at $B = 0$. While hysteretic $\delta f_0(\pm V,B)$ signal cannot be simply ascribed to a single source as both magnetoresistance and Hall conductivity have contributions from sample magnetization, the fact that the hysteresis profile is not entirely even or odd in $B$ suggests that both components are hysteretic. Finally, the $\delta f_0(\pm V,B)$ hysteresis coincided with the hysteresis in magnetization and its evolution with annealing, confirming that both the transport and magnetization hysteresis originate from the ITO.

### C. ITO Hall Bar Transport

To confirm our findings using Corbino disk torque magnetometry and highlight the power of the technique, we performed complementary measurements using a standard Hall bar configuration. For a given temperature, the sample was current-biased in the $x$-axis, and the longitudinal ($x$-axis) and transverse ($y$-axis) voltages were recorded as a function of $z$-axis magnetic field. Detection of the anomalous Hall effect in the transverse channel in such a configuration is difficult due to sample issues such as strong in-plane magnetic anisotropy and high sample resistance [15, 19, 20]. Negative magnetoresistance due to the reduction in spin-related scattering thus is typically used to relate transport to direct magnetization measurements in ITO. Hysteretic magnetoresistance would provide convincing evidence of ferromagnetism, pointing to the presence of magnetic domains that need to be flipped in direction when the magnetic field is reversed.

Initially resistive ITO was sputtered in a Hall bar pattern and successively annealed to detect the onset of magnetism. Note that Hall bar measurements were performed on more conductive ITO films of the same thickness as the Corbino disk samples due to the difficulties in measuring high resistance samples using a Hall bar technique. The $B = 0$ resistance was 15 k$\Omega/\square$ for the first anneal and 4.6 k$\Omega/\square$ for the second anneal. Relative magnetoresistance or $\delta R/R_0 \equiv [R(B) - R(0)]/R(0)$ for both anneals is shown in Fig. 8(a). More strongly annealed or conductive samples displayed more dramatic decreases in $\delta R/R_0$ at $|B| < 2$ T and asymptotic $\delta R/R_0$ for $|B| > 5$ T. The change in magnetoresistance to 7 T was $\approx -8$ % for both annealed samples. The amplitude and shape of the magnetoresistance curves are consistent with previous studies of ITO with changing carrier density and temperature [50]. Resistivity and carrier density of the Hall bar samples are included in Table I.

Hall effect and magnetoresistance data were further examined for evidence magnetism. Hysteretic magnetoresistance was found by comparing $\delta R/R_0$ during a magnetic field sweep up from -7 T to +7 T and sweep down from +7 T to -7 T. The average $\delta R/R_0$ during the up and down sweeps was then subtracted from each sweep $\delta R/R_0$ dataset to produce Fig. 8(b). Hysteretic magnetoresistance was observed below 2 T after annealing. The sign of hysteresis is consistent with previously observed in-plane magnetic ordering [5, 16, 51] and appeared only with annealing or increased granularity and carrier density. No hysteretic magnetoresistance was observed in the more lightly annealed dataset likely due to either increased magnetism with annealing or a lower slope in $\delta R/R_0$ near $B = 0$. No discernible anomalous Hall contribution could be detected, and the absence of AHE is consistent with strong in-plane magnetic anisotropy.

The Corbino disk cantilevers exhibit higher $B_s$ than the hysteresis-closing $B$ in the Hall bar samples shown in Fig. 8(b). The hysteresis closing field observed in the more annealed Hall bar ITO sample is approximately 2 T while all Corbino disk $B_s$ are $> 3$ T. Although magnetism is correlated with changes in granularity, after annealing there is no discernible difference in sample granularity between SEM images of the Hall bar and Corbino disk samples as seen in Fig. 9. Differences in sample microstructure thus do not explain the change in $B_s$ between sample geometries. Cantilever angle and strong $B_s$ anisotropy similarly does not account for differences in $B_s$. The applied $B$ for ITO on Corbino disk cantilevers includes an in-plane $B$ component due to cantilever bending. The ITO Hall bar was rotated by 20° from flat around the $x$-axis, where current is applied in the $x$-direction, to test for a strong in-plane field effect in $B_s$ and simulate a cantilever angle. The 20° angle magnetoresistance and hysteretic magnetoresistance data is included in Fig. 8. Any changes in $\delta R/R_0$ and $B_s$ with mounting angle were minimal and could be explained by slight differences in annealing between the flat and angle-mounted Hall bars. The difference in $B_s$ between the Corbino disk and Hall bar samples thus is not caused by an in-plane magnetic field with cantilever bending. The observed closing of the hysteresis loop in $\delta R/R_0$ at 2 T may instead result from the lower $dR/dB$ above 2 T. The hysteretic contribution to $\delta R/R_0$ from an effective offset in $B$ between the up and down magnetic field sweeps is proportional to $dR/dB$. The magnetic field at which the hysteresis loop in Fig. 8(b) closes corresponds to a decrease in the slope of $dR/dB$ in Fig. 8(a). Similarly, there was no observed hysteresis in the less annealed sample with a lower slope in $\delta R/R_0$ near $B = 0$. The high-field slope in $dR/dB$ therefore may not be high enough to observe hysteresis. The 2 T observed hysteresis loop closing field thus serves as a lower bound for $B_s$ in the Hall bar, with more direct measurements found through torque magnetometry.

## IV. CONCLUSIONS

We have shown unambiguous evidence of in-plane ferromagnetism and its effect on the transport properties of low carrier density ITO annealed through its MIT. Using a novel Corbino disk torque magnetometry technique [32], hysteresis in the voltage-independent shift in $f_0$ with $B$ provides a direct measurement of in-plane magnetic ordering, while at a finite voltage $\delta f_0(\pm V, B)$ exhibits AHE and hysteretic transport. In particular, the observation of AHE provides direct evidence of inherent magnetism in ITO. Examination of both the Hall and anomalous Hall contributions to $\delta f_0(\pm V, B)$ confirm the breaking of an in-plane magnetic ordering. Magnetism arose with annealing in ITO and thus with changes to the magnetic oxide morphology. The observation of intrinsic magnetism in ITO correlated with changes in surface morphology supports the hypothesis that magnetism arises from surface oxygen vacancies. Such Hall and magnetization measurements may be performed for deeply insulating materials due to the direct measurement of $\sigma_{xy}$. Initial results of $\sigma_{xy}$ in resistive ITO contradict expectations for both a Hall insulator and standard models of Mott variable range hopping [52–54]. Additionally, Corbino disk torque magnetometry provides the ability to simultaneously measure the bulk magnetic and transport properties of a material across the MIT, opening avenues for new physics.

## ACKNOWLEDGMENTS

This work was funded by Army Research Office grant W911NF1710588 in collaboration with Professor Amir Yacoby and by the Department of Energy, Office of Science, Basic Energy Sciences, Materials Sciences and Engineering Division, under Contract DEAC02-76SF00515.

### Appendix A: Grain Analysis

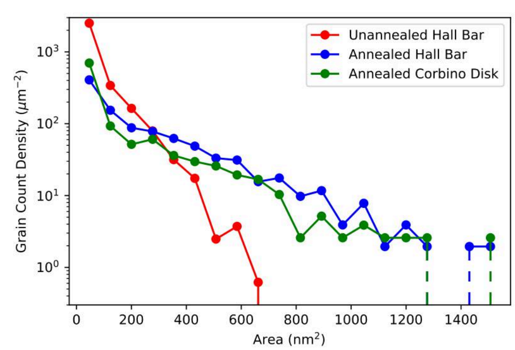


FIG. 9: Comparison of the grain sizes between the annealed and non-annealed ITO samples by SEM. Fluctuations in SEM brightness changed from local noise to distinct larger grains with annealing.

A comparison of the unannealed and annealed grain structure observed by SEM in Fig. 3 is shown in Fig. 9. Grains were identified by adaptive thresholding of the SEM images. The unannealed Hall bar shows evidence of only SEM noise which appears as very small grains. With further annealing, regular granularity is observed. The granularity of the Hall Bar and Corbino disk samples also become more similar after similar annealing treatment.

### Appendix B: Low Field $f_0$ Dependence

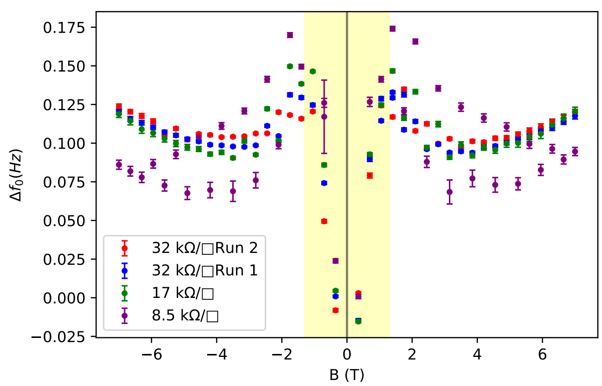


FIG. 10: Voltage-independent $\Delta f_0$ for four cooldowns. There is rapid increase in $\Delta f_0$ in the yellow highlighted region of $B$ near 0 T seen in all cooldowns regardless of sample magnetization. The low field $\Delta f_0$ is therefore not attributed to the ITO and is not fit in Fig. 5.

The full profile of $\Delta f_0$ with magnetic field for 4 annealing strengths is shown in Fig. 10. Hysteresis appears as fluctuations in $\Delta f_0$ between neighboring $B$ points when both sweep directions are plotted together. Without subtracting the background change in $f_0$ such hysteresis is most clear in the 8.5 kΩ sample.


[1] Y. Matsumoto, M. Murakami, T. Shono, T. Hasegawa, T. Fukumura, M. Kawasaki, P. Ahmet, T. Chikyow, S. ya Koshihara, and H. Koinuma, Room-temperature ferromagnetism in transparent transition metal-doped titanium dioxide, Science **291**, 854 (2001).

[2] S. B. Ogale, R. J. Choudhary, J. P. Buban, S. E. Lofland, S. R. Shinde, S. N. Kale, V. N. Kulkarni, J. Higgins, C. Lanci, J. R. Simpson, N. D. Browning, S. Das Sarma, H. D. Drew, R. L. Greene, and T. Venkatesan, High temperature ferromagnetism with a giant magnetic moment in transparent Co-doped $SnO_{2-\delta}$, Phys. Rev. Lett. **91**, 077205 (2003).

[3] P. Sharma, A. Gupta, K. V. Rao, F. J. Owens, R. Sharma, R. Ahuja, J. M. O. Guillen, B. Johansson, and G. A. Gehring, Ferromagnetism above room temperature in bulk and transparent thin films of Mn-doped ZnO, Nature Materials **2**, 673 (2003).

[4] A. Tiwari, V. M. Bhosle, S. Ramachandran, N. Sudhakar, J. Narayan, S. Budak, and A. Gupta, Ferromagnetism in Co doped $CeO_2$: Observation of a giant magnetic moment with a high curie temperature, Applied Physics Letters **88**, 142511 (2006).

[5] N. H. Hong, J. Sakai, N. T. Huong, and V. Brizé, Room temperature ferromagnetism in laser ablated Ni-doped $In_2O_3$ thin films, Applied Physics Letters **87**, 102505 (2005).

[6] G. Peleckis, X. Wang, and S. X. Dou, High temperature ferromagnetism in Ni-doped $In_2O_3$ and indium-tin oxide, Applied Physics Letters **89**, 022501 (2006).

[7] O. D. Jayakumar, I. K. Gopalakrishnan, S. K. Kulshreshtha, A. Gupta, K. V. Rao, D. V. Louzguine-Luzgin, A. Inoue, P.-A. Glans, J.-H. Guo, K. Samanta, M. K. Singh, and R. S. Katiyar, Structural and magnetic properties of $(In_{1-x}Fe_x)_2O_3$ (0.0≤x≤.25) system: Prepared by gel combustion method, Applied Physics Letters **91**, 052504 (2007).

[8] C.-Y. Park, S.-G. Yoon, Y.-H. Jo, and S.-C. Shin, Room-temperature ferromagnetism observed in Mo-doped indium oxide films, Applied Physics Letters **95**, 122502 (2009).

[9] M. Venkatesan, C. B. Fitzgerald, and J. M. D. Coey, Unexpected magnetism in a dielectric oxide, Nature **430**, 630 (2004).

[10] N. H. Hong, J. Sakai, N. Poirot, and V. Brizé, Room-temperature ferromagnetism observed in undoped semiconducting and insulating oxide thin films, Phys. Rev. B **73**, 132404 (2006).

[11] A. Sundaresan, R. Bhargavi, N. Rangarajan, U. Siddesh, and C. N. R. Rao, Ferromagnetism as a universal feature of nanoparticles of the otherwise nonmagnetic oxides, Phys. Rev. B **74**, 161306(R) (2006).

[12] J. Philip, N. Theodoropoulou, G. Berera, J. S. Moodera, and B. Satpati, High-temperature ferromagnetism in manganese-

doped indium–tin oxide films, Applied Physics Letters **85**, 777 (2004).

[13] T. Ohno, T. Kawahara, H. Tanaka, T. Kawai, M. Oku, K. Okada, and S. Kohiki, Ferromagnetism in transparent thin films of Fe-doped indium tin oxide, Japanese Journal of Applied Physics **45** (2006).

[14] M. Venkatesan, R. D. Gunning, P. Stamenov, and J. M. D. Coey, Room temperature ferromagnetism in Mn- and Fe-doped indium tin oxide thin films, Journal of Applied Physics **103**, 07D135 (2008).

[15] H. S. Kim, S. H. Ji, H. Kim, S.-K. Hong, D. Kim, Y. E. Ihm, and W. K. Choo, Observation of ferromagnetism and anomalous Hall effect in laser-deposited chromium-doped indium tin oxide films, Solid State Communications **137**, 41 (2006).

[16] A. M. H. R. Hakimi, F. Schoofs, M. G. Blamire, S. Langridge, and S. S. Dhesi, Intrinsic and extrinsic ferromagnetism in Co-doped indium tin oxide revealed using x-ray magnetic circular dichroism, Advances in Condensed Matter Physics **2017**, 2836254 (2017).

[17] H. S. Majumdar, S. Majumdar, D. Tobjörk, and R. Österbacka, Ferromagnetism in indium tin-oxide (ITO) electrodes at room temperature, Synthetic Metals **160**, 303 (2010), spins in Organic Semiconductors 2009, Salt Lake City, Utah, February 4-7.

[18] J. M. D. Coey, P. Stamenov, R. D. Gunning, M. Venkatesan, and K. Paul, Ferromagnetism in defect-ridden oxides and related materials, New Journal of Physics **12**, 053025 (2010).

[19] A. M. Hakimi, The quest for a dilute magnetic oxide, in *Magnetism and spin transport studies on indium tin oxide* (University of Cambridge, 2011) pp. 63–96.

[20] J. Stankiewicz, F. Villuendas, and J. Bartolomé, Magnetic behavior of sputtered Co-doped indium-tin oxide films, Phys. Rev. B **75**, 235308 (2007).

[21] L. F. Arsenault, B. Movaghar, P. Desjardins, and A. Yelon, Magnetotransport in the insulating regime of Mn-doped GaAs, Phys. Rev. B **78**, 075202 (2008).

[22] M. A. Paalanen, S. Sachdev, R. N. Bhatt, and A. E. Ruckenstein, Spin dynamics of nearly localized electrons, Phys. Rev. Lett. **57**, 2061 (1986).

[23] A. A. Burkov and L. Balents, Anomalous hall effect in ferromagnetic semiconductors in the hopping transport regime, Phys. Rev. Lett. **91**, 057202 (2003).

[24] N. M. Ahmed, F. A. Sabah, H. Abdulgafour, A. Alsadig, A. Sulieman, and M. Alkhoaryef, The effect of post annealing temperature on grain size of indium-tin-oxide for optical and electrical properties improvement, Results in Physics **13**, 102159 (2019).

[25] A. M. Hakimi, The indium oxide system, in *Magnetism and spin transport studies on indium tin oxide* (University of Cambridge, 2011) pp. 41–60.

[26] S. Song, T. Yang, J. Liu, Y. Xin, Y. Li, and S. Han, Rapid thermal annealing of ITO films, Applied Surface Science **257**, 7061 (2011).

[27] J. H. Lee, Y. H. Kim, S. J. Ahn, T. H. Ha, and H. S. Kim, Grain-size effect on the electrical properties of nanocrystalline indium tin oxide thin films, Materials Science and Engineering: B **199**, 37 (2015).

[28] L. Kerkache, A. Layadi, E. Dogheche, and D. Remiens, Annealing effect in DC and RF sputtered ITO thin films, http://dx.doi.org/10.1051/epjap:2007113 **39** (2007).

[29] D. Raoufi, A. Kiasatpour, H. Fallah, and A. Rozatian, Surface characterization and microstructure of ITO thin films at different annealing temperatures, Applied Surface Science **253**, 9085 (2007).

[30] M. Gulen, G. Yildirim, S. Bal, A. Varilci, I. Belenli, and M. Oz, Role of annealing temperature on microstructural and electro-optical properties of ITO films produced by sputtering, Journal of Materials Science: Materials in Electronics **24**, 467 (2013).

[31] W.-F. Wu and B.-S. Chiou, Effect of annealing on electrical and optical properties of RF magnetron sputtered indium tin oxide films, Applied Surface Science **68**, 497 (1993).

[32] S. Mumford, T. Paul, S. H. Lee, A. Yacoby, and A. Kapitulnik, A cantilever torque magnetometry method for the measurement of hall conductivity of highly resistive samples, Review of Scientific Instruments **91**, 045001 (2020).

[33] K. A. Modic, M. D. Bachmann, B. J. Ramshaw, F. Arnold, K. R. Shirer, A. Estry, J. B. Betts, N. J. Ghimire, E. D. Bauer, M. Schmidt, M. Baenitz, E. Svanidze, R. D. McDonald, A. Shekhter, and P. J. W. Moll, Resonant torsion magnetometry in anisotropic quantum materials, Nature Communications **9**, 3975 (2018).

[34] M. Perfetti, Cantilever torque magnetometry on coordination compounds: from theory to experiments, Coordination Chemistry Reviews **348**, 171 (2017).

[35] J. Chiaverini, K. Yasumura, and A. Kapitulnik, Microcantilever studies of angular field dependence of vortex dynamics in $Bi_2Sr_2CaCu_2O_{8-x}$, Phys. Rev. B **64**, 014516 (2001).

[36] A. C. Bleszynski-Jayich, W. E. Shanks, B. Peaudecerf, E. Ginossar, F. von Oppen, L. Glazman, and J. G. E. Harris, Persistent currents in normal metal rings, Science **326**, 272 (2009).

[37] E. Finot, A. Passian, and T. Thundat, Measurement of mechanical properties of cantilever shaped materials, Sensors **8**, 3497 (2008).

[38] O. M. Von Corbino, Phys. Z. **12**, 561 (1911).

[39] N. Manavizadeh, F. A. Boroumand, E. Asl-Soleimani, F. Raissi, S. Bagherzadeh, A. Khodayari, and M. A. Rasouli, Influence of substrates on the structural and morphological properties of RF sputtered ITO thin films for photovoltaic application, Thin Solid Films **517**, 2324 (2009), thin Film Chalogenide Photovoltaic Materials (EMRS, Symposium L).

[40] L. Friedman and M. Pollak, The Hall effect in the variable-range-hopping regime, Philosophical Magazine B **44**, 487 (1981).

[41] T. Holstein, Ann. Phys. (N.Y.) **8**, 343 (1959).

[42] O. Entin-Wohlman, A. G. Aronov, Y. Levinson, and Y. Imry, Hall resistance in the hopping regime: A "Hall insulator"?, Physical Review Letters **75**, 4094 (1995).

[43] O. Viehweger and K. B. Efetov, Phys. Rev. B **44**, 1168 (1991).

[44] S. Kivelson, D.-H. Lee, and S.-C. Zhang, Global phase diagram in the quantum Hall effect, Phys. Rev. B **46**, 2223 (1992).

[45] Y. Imry, Zero-temperature frequency-dependent Hall conductivity of the Anderson insulator, Phys. Rev. Lett. **71**, 1868 (1993).

[46] P. F. Hopkins, M. J. Burns, A. J. Rimberg, and R. M. Westervelt, Magnetic-field-induced localization in degenerately doped n-type Ge, Phys. Rev. B **39**, 12708 (1989).

[47] D. W. Koon and T. G. Castner, Hall effect near the metal-insulator transition, Phys. Rev. B **41**, 12054 (1990).

[48] E. Liu, Z. Huang, J.-G. Zheng, J. Yue, L. Chen, X. Wu, Y. Sui, Y. Zhai, S. Tang, J. Du, and H. Zhai, Texture induced magnetic anisotropy in $Fe_3O_4$ films, Applied Physics Letters **107**, 172403 (2015).

[49] R. M. Qiao, S. S. Yan, T. S. Xu, M. W. Zhao, Y. X. Chen, G. L. Liu, W. L. Yang, R. K. Zheng, and L. M. Mei, Anomalous hall effect in variable range hopping regime: Unusual scaling law and sign reversal with temperature (2014).

[50] A. Fujimoto, K. Yoshida, T. Higaki, Y. Kimura, M. Nakamoto, Y. Kashiwagi, M. Yamamoto, M. Saitoh, T. Ohno, and S. Fu-

ruta, Negative magnetoresistance of indium tin oxide nanoparticle thin films grown by chemical thermolysis, Journal of the Physical Society of Japan **82**, 024710 (2013).

[51] M. Majumder, M. Schmidt, H. Rosner, A. A. Tsirlin, H. Yasuoka, and M. Baenitz, Anisotropic $Ru^{3+}$ $4d^5$ magnetism in the alpha-$RuCl_3$ honeycomb system: susceptibility, specific heat, and zero-field NMR, Physical Review B **91**, 180401(R) (2015).

[52] R. Németh and B. Mühlschlegel, Hopping Hall conductivity in disordered and granular systems, Solid State Communications **66**, 999 (1988).

[53] D. Koon and T. Castner, Variable-range hopping and the hall coefficient in Si:As, Solid State Communications **64**, 11 (1987).

[54] M. Gruenewald, H. Mueller, P. Thomas, and D. Wuertz, The hopping hall mobility — A percolation approach, Solid State Communications **38**, 1011 (1981).